The Journal of Green Energy and Environmental Engineering

Research Paper

Molecular Dynamics Simulation of Nanocellulose Modified Cement-Based Materials

Fyodor Dostoevsky [1], Agatha Christie [2,*]

[1] Department of Management, Technology, and Economics, Swiss Federal Institute of Technology Zurich, Scheuchzerstrasse 7, 8092 Zurich, Switzerland
[2] Institute for Oral Biology, University of Klagenfurt, Klagenfurt, Austria
*Corresponding author: Fyodostoevsky@ethz.ch; Christie@uni-klu.ac.at

Abstract. Efforts to optimize the performance of cement-based matrices incorporating nanocellulose reinforcement are commonly constrained by the lack of clarity surrounding interfacial bonding mechanisms. In this work, molecular dynamics simulations at the atomistic level were carried out to systematically examine how the interface between calcium silicate hydrate (C–S–H) gel and nanocellulose is structured and behaves — covering its interfacial organization, molecular mobility, energetic characteristics, and mechanical response — with both unmodified and carboxyl-functionalized nanocellulose considered for comparison. Composite models with different surface functional groups were constructed by embedding nanocellulose into the C-S-H matrix. Simulation results reveal that the –COOH groups of carboxylated nanocellulose and –OH groups of hydroxylated nanocellulose provide abundant hydrogen bond sites for C-S-H gel. Interfacial binding energy is closely correlated with functional group types, and carboxylated nanocellulose exhibits remarkably higher interfacial binding energy than hydroxylated nanocellulose. In addition, the carboxyl modification introduces a larger population of non-bridging oxygen atoms, which are able to establish stable coordination with the calcium ions of C–S–H while simultaneously giving rise to a more densely interconnected hydrogen-bonding network. By clarifying at the atomic level how nanocellulose strengthens C–S–H gel, this work offers theoretical guidance and a rational basis for material selection in the development of high-performance, environmentally friendly cementitious composites.

Keywords: *nanocellulose; molecular dynamics simulation; cement-based materials; calcium silicate hydrate gel*

Received on 02 July 2025, Accepted on 05 Nov 2025, Published on 15 Dec 2025

1 Introduction

Over the preceding decade, the integration of nanoscale materials into cementitious matrices has garnered considerable scholarly interest. The inclusion of such nanomaterials has been demonstrated to markedly improve the compressive and flexural capacities, as well as the resistance to fracture, of cement-based systems. Derived from renewable biological feedstocks, nanocellulose is distinguished by the widespread availability of its precursors, its inherently sustainable nature, and its exceptional suite of physicochemical attributes, rendering it a highly promising candidate for advancing cementitious composite technologies. By providing anchoring points at which C–S–H gel can nucleate heterogeneously, the functional groups decorating nanocellulose surfaces steer hydration toward more compact products, and the pore network of the matrix is refined as a result. Earlier studies have likewise shown that adding nanocellulose to cement-based systems lowers the required amount of binder, thereby cutting the carbon dioxide footprint of construction and conforming to the sustainability goals that now steer the development of modern building materials. From a

mechanical standpoint, nanocellulose suppresses the propagation of microcracks through nanoscale void filling and fiber-bridging mechanisms, thereby cooperatively enhancing the mechanical integrity of cement matrices. Especially noteworthy is that the surfaces of nanocellulose are densely populated with hydroxyl groups and possess a remarkably large specific surface area, attributes that enable the formation of widespread hydrogen-bond networks with the products of cement hydration — C–S–H gel in particular. Such interfacial interactions not only significantly strengthen the interfacial bonding performance of composites, but also simultaneously boost ductility, toughness, impact resistance and flexibility.

Numerous scholars have conducted research on the performance improvement effect brought by nanocellulose. Hisseine et al. pointed out that adding nanocellulose can increase the load-bearing capacity and toughness of cement materials. Alrekabi et al. discovered that even a low dosage of nanocellulose can remarkably raise flexural strength and suppress microcrack extension. Investigations by Hoyos et al. and by Sun et al. revealed that introducing nanocellulose renders the cement matrix more compact and less porous, an effect that in turn reinforces the mechanical performance of the interfacial transition zone. Akhlaghi et al. and Bhalerao et al. further proposed that nanocellulose reinforces cement composites through nanofilling and microcrack bridging mechanisms. Nie Miaomiao found that when the mass fraction of nanocellulose reaches 0.2%, the fracture toughness of cement mortar is significantly improved. Deng Fangqian's research proved that appropriate nanocellulose doping can effectively elevate the cement hydration degree and microstructural compactness at interfaces, and homogenize elemental distribution. Huang Zhuolin confirmed that proper nanocellulose refines matrix pores via nanofilling and promotes uniform distribution of hydration products through bridging effects, so as to increase matrix compactness and shrinkage resistance.

Cement-based composites are influenced by numerous variables, yet none matters more for their ultimate mechanical response than the quality of adhesion between the reinforcing phase and the binder that surrounds it. Calcium silicate hydrate (C–S–H) gel, as the dominant hydration product, is the phase that ultimately dictates the strength and long-term durability of these systems. Gaining nanoscale insight into the interfacial region shared by nanocellulose and C–S–H gel therefore lays the groundwork for the deliberate, performance-oriented engineering of advanced cementitious materials. Nevertheless, limited by the observation difficulty at the nanoscale, traditional macroscopic material experiments and microscopic characterization techniques cannot directly characterize such interfacial behaviors, leading to insufficient understanding of the corresponding reinforcement mechanisms.

Further studies have proposed that the reinforcement effect of nanocellulose on cement matrices mainly originates from a dual microscopic mechanism of "short-circuit diffusion and microcrack bridging": the three-dimensional network of nanocellulose accelerates cement hydration while bridging microcracks, which may constitute the core mechanism for mechanical enhancement. To verify this hypothesis from a mechanistic perspective, molecular dynamics simulation was adopted in this work to establish composite models of nanocellulose and C-S-H, and investigate interfacial structures, mutual interactions and failure behaviors at the atomic scale.

Atomistic simulations have previously been employed in an effort to clarify how cellulose adheres to calcium silicate hydrate (C–S–H) at their shared interface. For instance, the work by Fan Qichang and colleagues established stratified composite architectures grounded in the Tobermorite crystalline framework and quantified the adsorption energies at the interface; nevertheless, their investigation did not address the binding phenomena occurring at the C–S–H/amorphous cellulose boundary. Motivated by the issues outlined above, this work puts forward a new molecular dynamics framework in which Monte Carlo sampling is used to assemble cellulose/C–S–H composite models that embed cellulose within structurally realistic C–S–H matrices. Mechanical stress–strain behaviors, interfacial energetic profiles, temporal evolution of hydrogen-bonding networks, and degradation and failure modes at the interface were subjected to comprehensive scrutiny, with the objective of illuminating the strengthening mechanism by which nanocellulose reinforces cementitious matrices.

2 Model Construction

Occupying an estimated 60–70% of the volume of all hydration products, calcium silicate hydrate (C–S–H) gel functions as the principal phase responsible for binding in cementitious systems. The way this gel is organized at the nanoscale, together with its mechanical behavior at the mesoscale, essentially determines how cementitious matrices perform at the macroscopic level, including their ability to bond with foreign materials. C-S-H presents a typical layered-particle composite configuration composed of short-range ordered Ca-O layers, randomly stacked silicate tetrahedral chains, interlayer free calcium cations and water molecules. The multiphase heterogeneity and topological disorder of C-S-H affect ion transport channels, mechanical strength and micro-pore distribution in hardened pastes, and thus become the core factors governing strain hardening, impermeability and crack resistance of cement materials.

2.1 Construction of C-S-H Model

To probe how cellulose fibers adhere to C–S–H at their interface, we adopted the molecular-scale model of Pellenq et al., whose composition $(CaO)_{1.65}(SiO_2)(H_2O)_{1.75}$ falls squarely within the experimentally established window for C–S–H — namely a density near 2.6 g/cm³ and Ca/Si molar ratios between 1.6 and 1.8, as verified by NMR, TEM, and SANS measurements. Relaxation of the atomic positions through grand canonical Monte Carlo (GCMC) sampling then yielded a configuration whose structure reproduces these experimental observations with high fidelity. In contrast to conventional crystal-based representations such as 11 Å Tobermorite, the Pellenq structure captures far more faithfully the spatial heterogeneity and topological disorder characteristic of C–S–H in real cement pastes.

The modeling procedure was implemented in the following sequence. The 11 Å Tobermorite crystal, whose Ca/Si molar ratio is 0.75, served as the initial template and was expanded into orthogonal supercells. To bring the composition closer to that of genuine C–S–H, silicate tetrahedra occupying mid-chain or terminal sites along the silicate chains were randomly removed, giving rise to defective, water-free calcium silicate skeletons. The model was saturated with water at room temperature (298 K) to obtain water-filled C-S-H specimens, and the full modeling workflow is illustrated in Figure 1.

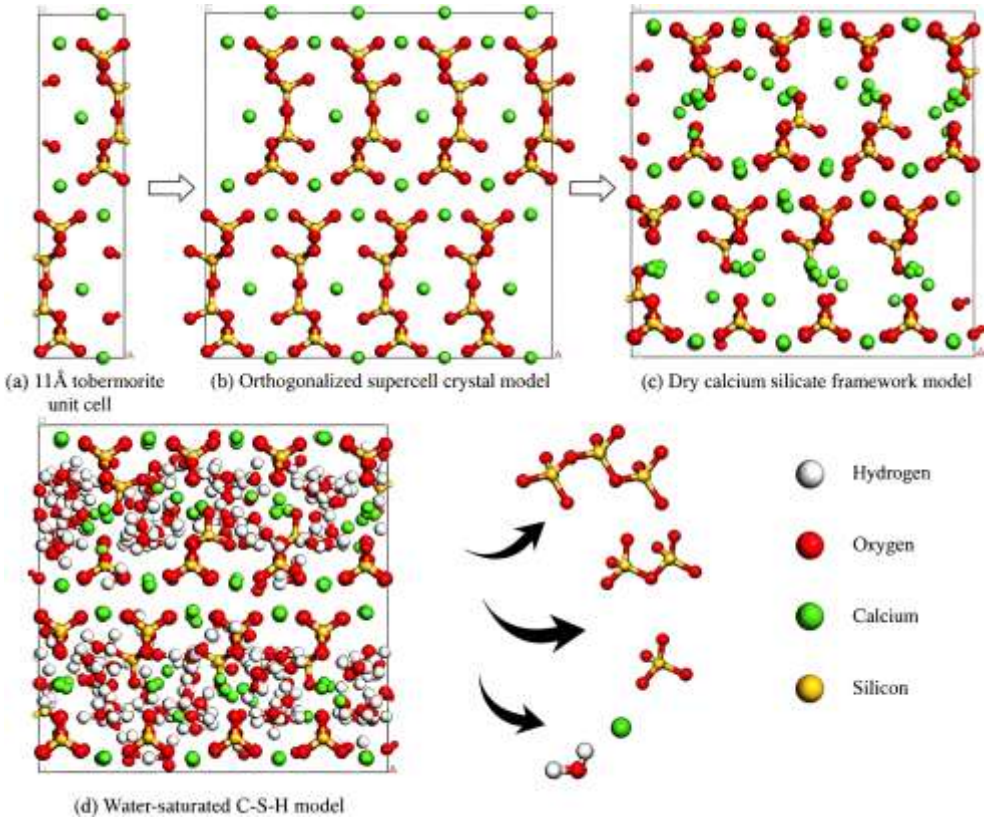

Figure 1 Modeling Process of C-S-H Note: White = Hydrogen; Red = Oxygen; Green = Calcium; Yellow = Silicon (a) 11 Å tobermorite unit cell; (b) Orthogonalized supercell crystal model; (c) Dry calcium silicate framework model; (d) Water-saturated C-S-H model

Multi-step energy optimization and dynamic relaxation were conducted on the model. First, system potential energy was minimized, and charge distribution was calculated via the charge equilibration (QEq) method to ensure self-consistency between atomic charges and force field parameters. Afterwards, molecular dynamics optimization under the NPT ensemble was carried out with the COMPASS force field: temperature maintained at 298 K, simulation duration of 120 ps, time step of 1 fs. Such dynamic relaxation eliminates internal stress of initial configurations and brings the system to thermodynamic equilibrium, meeting the requirements for subsequent analytical work.

2.2 Construction of Cellulose Model

Existing literature demonstrates that natural cellulose consists mainly of two crystalline phases (I_a and I_β) and amorphous regions. Mechanical or chemical treatments during cellulose preparation often destroy crystalline zone structures. An amorphous cellulose configuration was adopted in this work so as to probe its interaction with C–S–H in greater detail. The fundamental repeating unit of cellulose is cellobiose, whose molecular structure is depicted in Figure 2.

The fundamental cellulose repeat unit, \((C_{6}H_{10}O_{5})\), comprising 12 carbon, 10 oxygen, and 22 hydrogen atoms, was first assembled in the simulation package, with O_5 designated as the head atom and C4 as the tail atom (Figure 3). On this basis, chains of 20 linked repeat units were generated and subsequently subjected to geometry optimization within the COMPASS force field, using an energy convergence criterion of 0.001 kcal/mol. A three-dimensional periodic cell with dimensions of \(43.0 \AA ×43.0 \AA\) was established, and five cellulose chains were randomly filled into the cell via GCMC to form initial configurations (Figure 4). NVT ensemble dynamic relaxation (298 K, 100 ps, 1 fs time step) was then performed to eliminate internal residual stress.

Validation of the model rests on two observations: its calculated density of 1.32 g/cm³ matches values measured experimentally, and the system's energy remained stable, with fluctuations kept under 5% throughout the simulation. The mismatch of cell edge lengths between cellulose and pre-built C-S-H models was less than 5%, laying a solid foundation for subsequent interfacial interaction research.

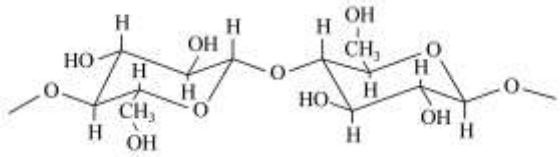

Figure 2 Cellulose repeating unit composed of two β-D-glucopyranose rings Note: Gray = Carbon; Red = Oxygen; White = Hydrogen

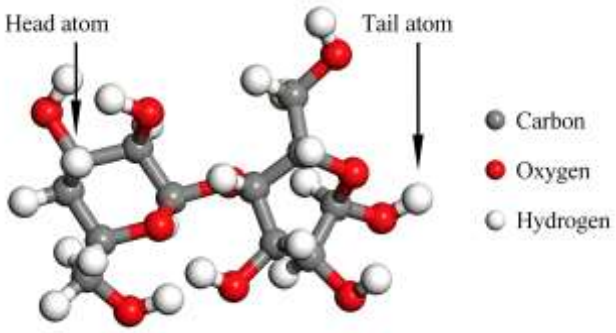

Figure 3 Monomer modeling diagram of cellulose, marking head atom and tail atom

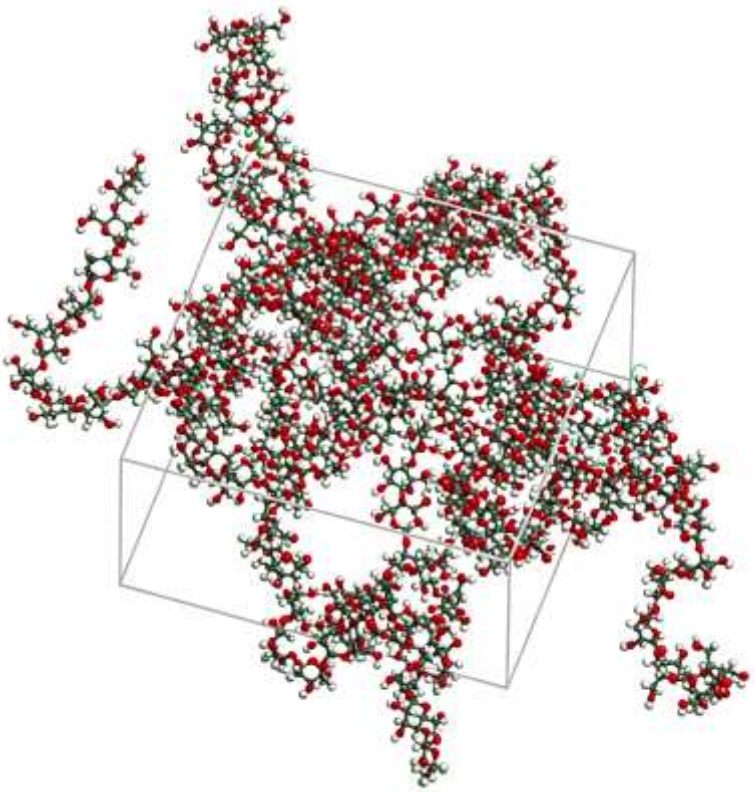

Figure 4 Cellulose unit cell constructed via Atmosphere Cell module

2.3 Construction of C-S-H/Cellulose Composite Model

A multi-scale modeling approach was adopted to resolve the atomic matching challenge at amorphous-crystalline interfaces and build C-S-H/cellulose composite systems. Based on pre-optimized C-S-H cells (density: 2.45 g/cm³) and amorphous cellulose models, a cubic simulation box with a size of \(43 \AA ×43 \AA ×120 \AA\) was established. The amorphous cellulose cell was inserted into interlayers of C-S-H, and a 5 Å vacuum layer was reserved to prevent initial atomic overlap (Figure 5a). Geometric optimization and molecular dynamics relaxation were carried out prior to formal MD simulation to stabilize the energy of initial configurations.

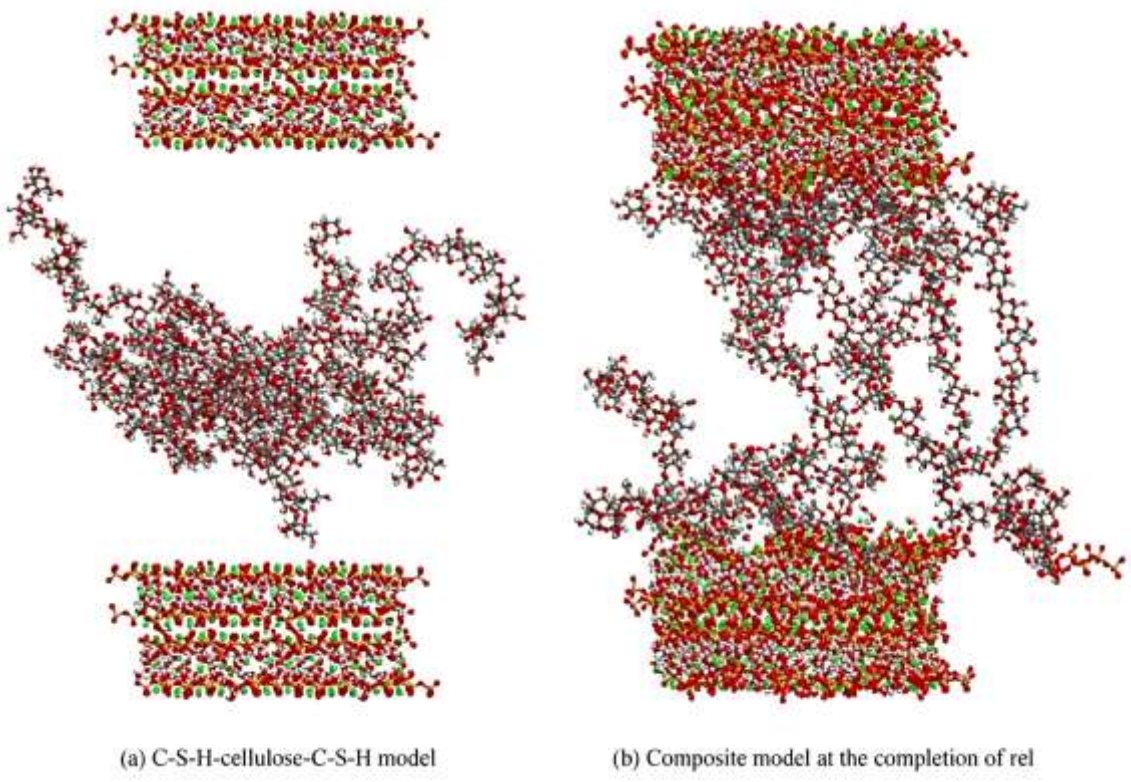

Figure 5 Composite model before and after relaxation (a) Unrelaxed C-S-H-cellulose-C-S-H sandwich model (b) Composite model after complete dynamic relaxation

First, geometric optimization was performed to minimize potential energy. Geometry relaxation was performed by combining three minimization schemes — steepest descent, conjugate gradient, and Newton–Raphson — applied in succession until the energy change fell below 1.0×10^{-4} kcal/mol and the residual force dropped under 0.001 kcal/(mol·Å). This procedure relieves the starting configuration of unfavorable atomic overlaps and distorted bonding. Thereafter, the structure was brought to thermodynamic equilibrium through a 100 ps NVT run at 298 K, advanced in 1 fs increments; the resulting fully relaxed composite configuration is displayed in Figure 5b.

3 Results and Discussion

Molecular dynamics simulations at the atomic scale were carried out to clarify how carboxyl-functionalized cellulose (Cellulose-COOH) and hydroxyl-terminated cellulose (Cellulose-OH) bind to calcium silicate hydrate (C–S–H) gel at their shared interface, and to assess how these interfacial interactions translate into the macroscopic mechanical properties of the resulting composites. The calculations demonstrate that grafting carboxyl groups onto cellulose substantially reinforces its adhesion to C–S–H, which in turn improves the composite's overall performance. In what follows, the mechanisms behind this reinforcement are examined in detail from three complementary angles.

3.1 Analysis of C-S-H Models

A series of C–S–H structures with Ca/Si ratios of 0.75, 1.31, 1.48, and 1.67 was generated to probe the mechanical response of the gel; each ratio was realized by selectively excising silicate tetrahedra so as to shorten the silicate chains. Figure 6 illustrates this principle: cutting out bridging tetrahedra fragments the long chains and, as a consequence, raises the Ca/Si ratio. Following the convention put forward by Pellenq, silicon speciation is described by Q_n notation, where the subscript *n* counts the bridging oxygens attached to a given silicon — Q_0 refers to isolated monomeric tetrahedra, Q_1 to tetrahedra located at chain termini, and Q_2 to those

embedded within extended chains. The fractional distribution of these Q_n units in the model at Ca/Si = 1.67 is given in Figure 7.

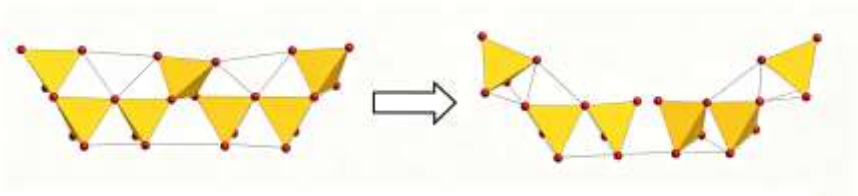

Figure 6 Schematic diagram of short silicate chain formation

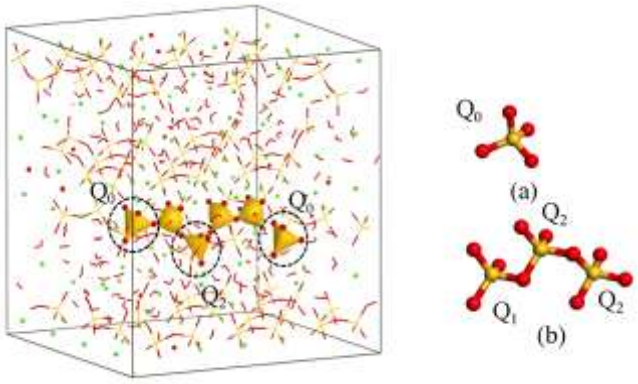

Figure 7 Various types of Qn units in C-S-H model (Ca/Si=1.67) (a) Isolated Q0 tetrahedron; (b) Chain segments composed of Q1 and Q2 units

Table 1 Variation of Q0, Q1, Q2 contents with different Ca/Si ratios

Ca/Si Ratio	Q_0 / %	Q_1 / %	Q_2 / %	Atomic Number (Ca/Si/H)	Density / ($g \cdot cm^{-3}$)
0.75	0.00	0.00	100.00	108 / 144 / 112	2.40
1.31	0.01	60.00	38.10	144 / 110 / 168	2.50
1.48	0.00	71.60	25.30	141 / 95 / 144	2.30
1.67	11.60	65.12	20.00	144 / 86 / 290	2.44

The C-S-H model constructed via Monte Carlo method with Ca/Si=1.67 achieves a final density of 2.44 g/cm³, with silicate chain distribution of Q0=11.6%, Q1=65.12%, Q2=20%, consistent with real C-S-H gel molecular models. As the Ca/Si ratio rises from 0.75 to 1.67, the polymerization degree of silicate tetrahedral structures gradually decreases regularly.

3.2 Uniaxial Tensile Simulation

Tensile deformation along a single axis was simulated for the unmodified C–S–H gel and for both C–S–H/polymer composite configurations. Before loading, each C–S–H structure was relaxed for 100 ps in the NVT ensemble at 298 K, with the pressure along all three Cartesian directions kept at zero; temperature control relied on the Berendsen thermostat, and the equations of motion were integrated with the Verlet scheme using a 1 fs step. Taking Z-direction stretching as the representative case, strain was imposed incrementally along Z while the normal stresses on the X and Y planes were released to zero, thereby allowing lateral contraction (the Poisson effect). From the stress–strain curves obtained in this way, two stiffness-related quantities — the elastic modulus and the fracture strength — were extracted.

These two parameters, both directly readable from the stress–strain response, serve as the primary indicators of the mechanical quality of C–S–H gel. Figure 9a compares the tensile stress–strain curves recorded along the Z-axis for the three model systems. Because the gel's cohesion relies heavily on relatively weak hydrogen bonds, tensile failure occurs most readily in the Z-direction. For the analyses that follow, the C–S–H structure with Ca/Si = 1.67 is adopted throughout.

When stretched along the Z-axis, the C–S–H gel responds in a three-stage fashion: the stress first rises steeply to a maximum of 0.99 GPa at a strain of 0.1, then gradually decays to 0.69 GPa by the time the strain attains 0.32, and finally plummets to zero once the strain reaches 0.6. This sharp post-peak drop in load-bearing capacity reflects the inherently brittle character of the gel in the direction perpendicular to its layers.

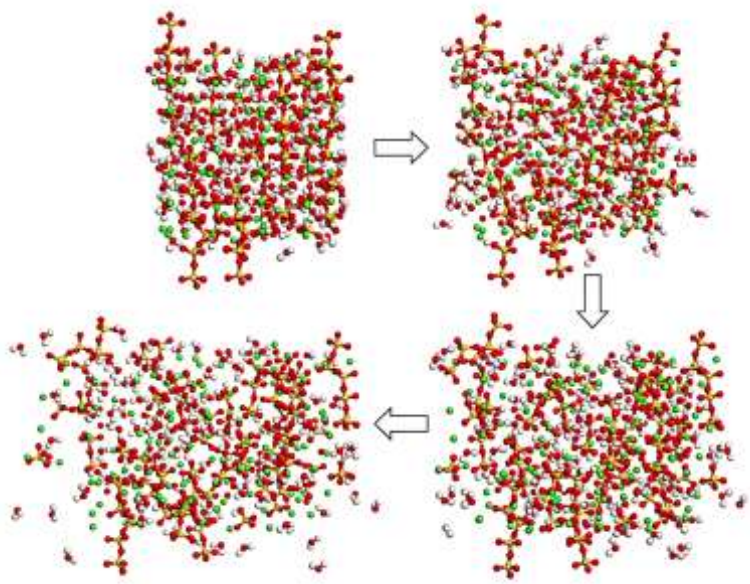

Figure 8 Snapshots of C-S-H during extension

Loading simulations along the three crystallographic directions (X, Y, and Z) expose a strong directional dependence of the mechanical properties. The weakest response — in terms of both tensile strength and modulus — occurs along Z, the axis normal to the silicate sheets, while markedly higher values are recorded within the X–Y plane. As the Ca/Si ratio increases, Young's modulus falls steadily in all three directions, consistent with the observations of Abdolhosseini Qomi and co-workers. At Ca/Si = 1.67, the calculated moduli lie between 10 and 30 GPa depending on the axis, matching nanoindentation data reported for laboratory-synthesized C–S–H gels. The modulus measured along Y invariably exceeds those along X and Z, a difference attributable to the fact that deformation along Y is resisted mainly by the covalent backbones of the silicate chains, whereas resistance along X and Z stems from hydrogen-bond networks that are weaker and partly interrupted. These results point to a compositional route — adjustment of Ca/Si — for rationally tuning the bulk mechanical performance of cement-based materials.

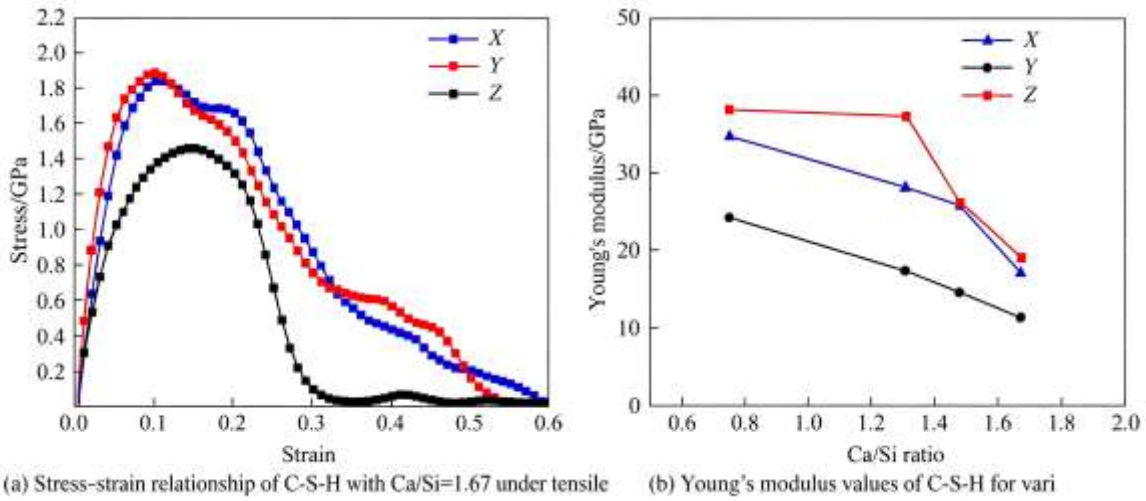

Figure 9 Mechanical characteristics of the C–S–H gel phase. (a) Uniaxial tensile stress–strain profile for C–S–H with Ca/Si = 1.67. (b) Dependence of Young's modulus on Ca/Si ratio along the principal X, Y, and Z crystallographic directions.

3.3 Interfacial Interactions

The interfacial configuration and dynamic behaviors of nanocomposites strongly depend on the interaction characteristics between polymer fillers and matrices. Interfacial binding energy combined with radial distribution function (RDF) was analyzed to evaluate the interaction intensity between cellulose before and modification and C-S-H, as well as atomic stacking and bonding environments at interfaces. Combined analysis of the two indicators elaborates the intrinsic mechanism of conformational variations observed in composite models.

3.3.1 Interfacial Interaction Energy

In fiber-reinforced composite systems, interfacial performance between fibers and matrices is co-regulated by interaction energy and hydrogen bond networks, which together determine interfacial bonding strength and macroscopic mechanical behaviors. To comprehensively elucidate the boundary characteristics at the nanocellulose–calcium silicate hydrate interface, quantitative assessments of interfacial binding energies together with hydrogen bond populations were systematically executed.

The strength of interfacial adhesion was quantified as the difference between the potential energy of the fully assembled composite and the sum of the potential energies of its two constituents considered separately, according to Equation (1): $E_{inter}= E_{total} - E_{C\text{-}S\text{-}H}+ E_{CNF}$, Where: E_{inter} = interfacial interaction energy; E_{total} = total potential energy of composite system; $E_{C\text{-}S\text{-}H}$ = potential energy of independent C-S-H model; E_{CNF} = potential of independent nanocellulose model.

Table 2 Simulation results of interfacial interaction energy for two cellulose/C-S-H composite models

Model	E_{total} / (10^2 kJ·mol^{-1}	$E_{C\text{-}S\text{-}H}$ / (10^2 kJ·mol^{-1})	E_{CNF} / (10^2 kJ·mol^{-1})	E_{inter} / (10^2 kJ·mol^{-1})
C-S-H-CNF_{oh}	–668.02	–690.97	23.67	–0.73
C-S-H-CNFCOOH	–679.09	–690.22	12.83	–1.70

Data in Table 2 show that the interfacial interaction energy of both composite systems is negative. In molecular dynamics simulation, \(E_{inter}<0\) indicates that the total energy of the composite system is lower than the sum of isolated components, energy is released when the two phases combine, and spontaneous interfacial

adsorption occurs to form thermodynamically stable structures. Comparative analysis reveals that the carboxyl-functionalized cellulose/C–S–H system registers a greater magnitude of interfacial interaction energy relative to its hydroxyl-terminated counterpart, thereby substantiating a more thermodynamically favorable spontaneous adsorption process and a more cohesive interfacial junction. These findings indicate that the chemical identity of surface functional moieties serves as a critical determinant governing the binding characteristics at the nanocellulose–C–S–H boundary. Negative interaction energy confirms spontaneous adsorption between the two materials driven by non-covalent forces.

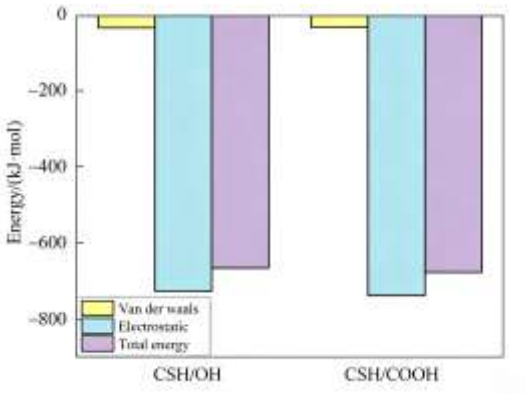

Figure 10 Bar chart comparison of van der Waals energy, electrostatic energy and total interfacial energy for C-S-H/OH and C-S-H/COOH systems

The distribution of hydrogen bonds across the three regions — the interior of the C–S–H phase, the cellulose domain, and the transition zone lying between them — is mapped in Figure 11. At this boundary, the cellulose chains establish hydrogen bonds with oxygen and hydrogen atoms contributed by water molecules, hydroxyl groups, and silicate tetrahedra belonging to the gel, and it is this bonding that strengthens interfacial adhesion. Because carboxylated cellulose presents an even greater density of hydroxyl functionalities, it engages C–S–H in a larger number of hydrogen bonds, which translates into a higher interfacial interaction energy.

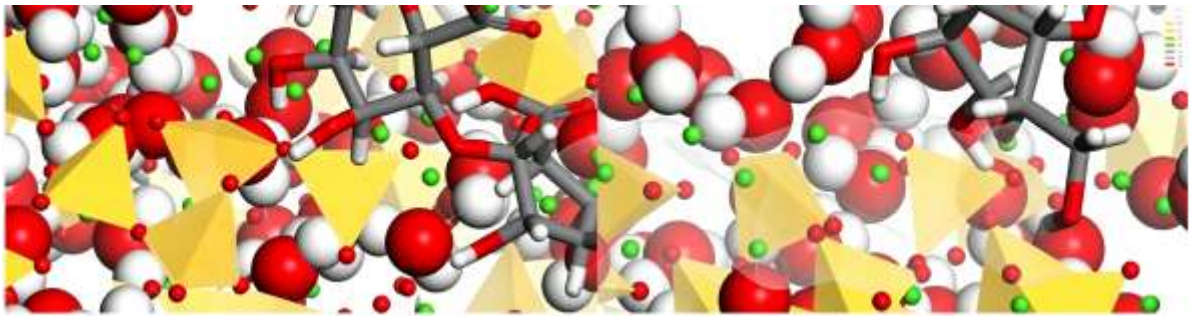

Figure 11 Distribution diagram of hydrogen bonds in the model (blue dotted lines are hydrogen bonds)

Hydrogen bond statistics reveal that the interface of carboxylated cellulose/C-S-H composite model forms 56.1 hydrogen bonds, equivalent to a hydrogen bond density of 3.12 bonds per square nanometer. In contrast, the hydroxylated cellulose/C-S-H interface only generates 25.7 hydrogen bonds with a density of 1.43 bonds/nm², far lower than the carboxylated group system. It is concluded that hydrogen bonds can strengthen interfacial linkage and enhance mutual interactions between two phases.

3.3.2 Radial Distribution Function (RDF) & Mean Squared Displacement (MSD)

The interfacial behavior of the nanocellulose/C–S–H composites was characterized by means of radial distribution function (RDF) and mean square displacement (MSD) analyses, offering complementary perspectives on the boundary region: the former resolves how atoms are arranged and bonded across the interface, while the latter captures the extent of atomic mobility there.

According to Sanchez's research, the cut-off distance for hydrogen bonds is generally 2.5 Å. RDF curves within the 0~5 Å range were analyzed based on this standard. Peaks near 1 Å correspond to O-H covalent bonds of hydroxyl groups, while peaks between 1.25~2.5 Å are attributed to hydrogen bond formation.

As shown by the RDF curves in Figure 12, the oxygen and hydrogen atoms contributed by the C–S–H phase give rise to pronounced peaks at 0.97 Å and 2.05 Å, respectively; since both separations fall short of the 2.5 Å cutoff customarily used to define a hydrogen bond, they confirm hydrogen-bond formation at the interface. Notably, the carbonyl oxygen atoms (O=C) within the carboxyl functionalities manifest more pronounced spatial correlations with neighboring hydrogen atoms, as evidenced by their substantially sharper and more intense peak features. This observation points to a markedly enhanced propensity of carboxyl-bound oxygen for participating in hydrogen-bonding interactions at the interface, relative to other oxygen species present in the system.

MSD quantifies the average offset of all atoms relative to their initial positions during simulation; larger MSD values represent more intense atomic motion and weaker binding constraints. MSD values of Ca, Si and O atoms in C-S-H gel within 500 ps were analyzed for different interfaces (Figure 13). According to the MSD results, atoms located at the boundary between C–S–H and hydroxyl-functionalized cellulose undergo considerably smaller displacements than those residing at the interface with carboxylated cellulose — an indication that their motion is more strongly restricted and their diffusion correspondingly suppressed.

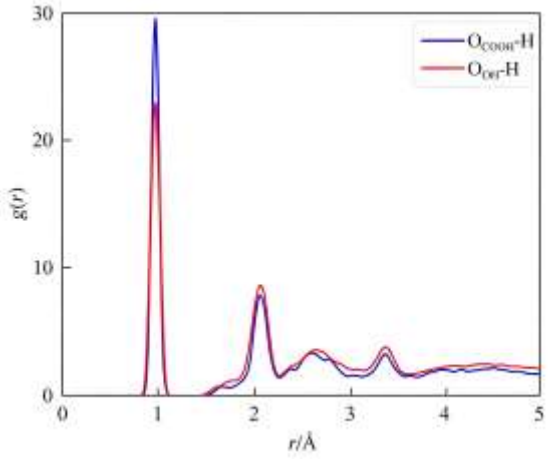

Figure 12 Radial distribution function curves of interfacial atoms for two composite systems

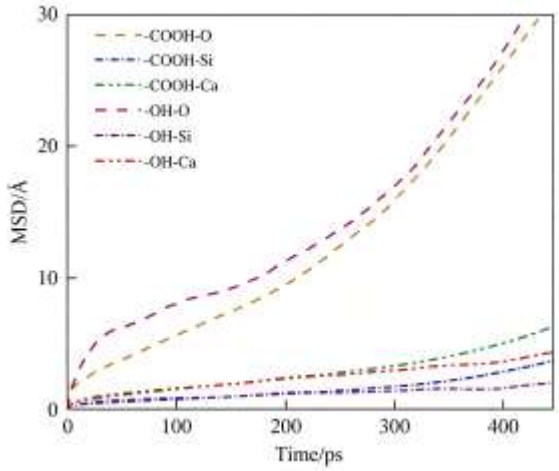

Figure 13 MSD evolution curves of interfacial atoms over simulation time

This result matches the interfacial adsorption energy data mentioned above. The C-S-H/carboxylated cellulose interface with stronger adsorption energy forms denser hydrogen bonds and chemical interactions, which lock surface atoms of C-S-H more firmly around nanocellulose. Restricted atomic mobility improves interfacial structural stability, enabling efficient stress transfer from matrices to reinforcing phases under external loads. Improved interfacial stability serves as the fundamental reason for enhanced macroscopic mechanical and durability performance of composite mortar.

By comparing the interfacial energy of different composite systems, it is verified that carboxylated cellulose possesses far stronger interfacial binding capacity with C-S-H than ordinary hydroxylated cellulose. Such reinforced interfacial interactions directly translate into superior macroscopic mechanical properties of composites, including higher tensile strength, elastic modulus and fracture energy. This atomic-scale simulation confirms that carboxylation modification of biomass cellulose is a promising strategy to greatly improve the interfacial and mechanical performance of cement-based composite materials.

4 Conclusions

Atomistic molecular dynamics simulations were systematically employed to scrutinize the interfacial structural features, energetic evolution, hydrogen-bonding network patterns, and mechanical response characteristics of calcium silicate hydrate/nanocellulose composite systems. The principal inferences drawn from this investigation are consolidated as follows:

A C–S–H structure having a Ca/Si ratio of 1.67 was assembled through Monte Carlo sampling; it exhibits a density of 2.44 g/cm³ together with silicate speciation of Q_0 = 11.6%, Q_1 = 65.12%, and Q_2 = 20%, closely mirroring the molecular makeup of genuine C–S–H gels. Raising the Ca/Si ratio from 0.75 to 1.67 progressively depolymerizes the silicate chains, and this structural change is accompanied by a corresponding reduction in the gel's elastic modulus along each of the X, Y, and Z axes.

Where nanocellulose meets C–S–H, attachment takes place spontaneously and is thermodynamically downhill. The surface groups of nanocellulose engage in hydrogen bonding with the surrounding water, hydroxide species, and the hydrogen and oxygen atoms of the silicate tetrahedra, an interaction network that tightens the contact between the two phases. This bonding is far more extensive at the interface involving carboxylated cellulose than at the one formed with hydroxylated cellulose.

Reinforcement of the C–S–H matrix is achieved with nanocellulose in either its pristine or carboxyl-functionalized form, yet the two differ in strength of attachment: the interface involving carboxylated nanocellulose reaches a binding energy of roughly -1.70×10^2 kJ/mol, substantially larger in magnitude than that recorded for its hydroxyl-only analogue. The overall adhesive energy is predominantly governed by van der Waals attractions and electrostatic forces, with the latter accounting for in excess of 90% of the total adsorption energy. This pronounced electrostatic dominance indicates that surface carboxylation confers substantially more effective interfacial reinforcement than the pristine hydroxyl-terminated configuration.

References

[1] Huang C L, Wang D M, Bai Y F. Review on Application of Nanocrystalline Cellulose in Cement-Based Mater ials[J]. Materials Reports, 2018, 32(z1): 462–465.

[2] Trache D, Tarchoun A F, Abdelaziz A, et al. A comprehensive review on processing, characteristics, and ap plications of cellulose nanofibrils/graphene hybrid-based nanocomposites: Toward a synergy between tw o-star nanomaterials[J]. International Journal of Biological Macromolecules, 2024, 268: 131633.

[3] Al-Askary A S J, Kopecskó K, Oktay D. Cellulose nanocrystals and their utilization in cement-based composi tes: A comprehensive review[J]. Case Studies in Construction Materials, 2025, 23: e05550.

[4] Hisseine O A, Wilson W, Sorelli L, et al. Nanocellulose for improved concrete performance: A macro-to-mi cro investigation for disclosing the effects of cellulose filaments on strength of cement systems[J]. Constr uction and Building Materials, 2019, 206: 84–96.

[5] Alrekabi S, Cundy A B, Lampropoulos A, et al. Mechanical performance of novel cement-based composite s prepared with nano-fibres, and hybrid nano- and micro-fibres[J]. Composite Structures, 2017, 178: 145–156.
[6] Gómez Hoyos C, Cristia E, Vázquez A. Effect of cellulose microcrystalline particles on properties of cement based composites[J]. Materials & Design, 2013, 51: 810–818.
[7] Sun X X, Wu Q L, Lee S, et al. Cellulose nanofibers as a modifier for rheology, curing and mechanical perfo rmance of oil well cement[J]. Scientific Reports, 2016, 6: 31654.
[8] Akhlaghi M A, Bagherpour R, Kalhori H. Application of bacterial nanocellulose fibers as reinforcement in c ement composites[J]. Construction and Building Materials, 2020, 241: 118061.
[9] Bhalerao N, Wayal A S, Patil P G. A review on effect of nano cellulose on concrete[J]. International Journal of Civil Structural Engineering Research, 2015, 3(1): 251–254.
[10] Nie M M. Research on the mechanical properties of cement-based materials modified with nanofibrillate d cellulose[D]. Jinan: Shandong Jianzhu University, 2023.
[11] Deng F Q, Tang K, Cao C, et al. Microstructural characterization of aggregate-matrix interface of recycled c oncrete modified by nanocellulose[J]. Cement, 2024(11): 8–13.
[12] Huang Z L, Tian D M, Yin J, et al. Influence and mechanism of nanocellulose on shrinkage performance of UHPC[J]. Journal of Railway Science and Engineering, 2025, 22(12): 5389–5397.
[13] Cao Y Z, Zavatterri P, Youngblood J. The influence of cellulose nanocrystal additions on the performance o f cement paste[J]. Cement and Concrete Composites, 2015, 56: 73–83.
[14] Zhang J, Liu Q L, Zhang J. Research on shrinkage and deformation performance of nanocellulose modified cement mortar[J]. Concrete, 2025(3): 172–176.
[15] Fan Q C, Wang Z P, Meng X. Molecular dynamics simulation and experimental study of cellulose nanocrys tal reinforced cement composites[J]. Acta Materiae Compositae Sinica, 2023, 40(9): 5315–5329.
[16] Basquiroto de Souza F, Sagoe-Crentsil K, Duan W H. A century of research on calcium silicate hydrate (C–S –H): Leaping from structural characterization to nanoengineering[J]. Journal of the American Ceramic Soci ety, 2022, 105(5): 3081–3099.
[17] Masoumi S, Ebrahimi D, Valipour H. Nanolayered attributes of calcium-silicate-hydrate gels[J]. Journal of t he American Ceramic Society, 2020, 103(1): 541–557.
[18] Bauchy M, Qomi M J A, Bichara C. Rigidity transition in materials: Hardness is driven by weak atomic cons traints[J]. Physical Review Letters, 2015, 114(12): 125502.
[19] Pellenq R J M, Kushima A, Shahsavari R. A realistic molecular model of cement hydrates[J]. Proceedings of the National Academy of Sciences of the United States of America, 2009, 106(38): 16102–16107.
[20] Cong X D, Kirkpatrick R J. ^{17}O and ^{29}Si MAS NMR study of β–C_2S hydration and the structure of calcium-silic ate hydrates[J]. Cement and Concrete Research, 1993, 23(5): 1065–1077.
[21] Nishiyama Y, Langan P, Chanzy H. Crystal structure and hydrogen-bonding system in cellulose Iβ from syn chrotron X-ray and neutron fiber diffraction[J]. Journal of the American Chemical Society, 2002, 124(31): 9074–9082.
[22] Ioelovich M. Preparation, characterization and application of amorphized cellulose: A review[J]. Polymers, 2021, 13(24): 4313.
[23] Mazeau K, Heux L. Molecular dynamics simulations of bulk native crystalline and amorphous structures of cellulose[J]. The Journal of Physical Chemistry B, 2003, 107(10): 2394–2403.
[24] Chen W, Lickfield G C, Yang C Q. Molecular modeling of cellulose in amorphous state. Part I: Model buildi ng and plastic deformation study[J]. Polymer, 2004, 45(3): 1063–1071.
[25] Chen J J, Thomas J J, Taylor H F W. Solubility and structure of calcium silicate hydrate[J]. Cement and Conc rete Research, 2004, 34(9): 1499–1519.
[26] Ramasamy J, Amanullah M. Nanocellulose for oil and gas field drilling and cementing applications[J]. Jour nal of Petroleum Science and Engineering, 2020, 184: 106292.
[27] Sanchez F, Zhang L. Molecular dynamics modeling of the interface between surface functionalized graphit ic structures and calcium–silicate–hydrate: Interaction energies, structure, and dynamics[J]. Journal of Col loid and Interface Science, 2008, 323(2): 349–358.
[28] Abdolhosseini Qomi M J, Krakowiak K J, Bauchy M. Combinatorial molecular optimization of cement hydr ates[J]. Nature Communications, 2014, 5: 4960.
[29] Hou D S, Zhao T J, Ma H Y. Reactive molecular simulation on water confined in the nanopores of the calciu m silicate hydrate gel: Structure, reactivity, and mechanical properties[J]. The Journal of Physical Chemist ry C, 2015, 119(3): 1346–1358.

[30] Hou D S, Zhao T J, Jin Z Q. Molecular simulation of calcium silicate composites[J]. Journal of the American Ceramic Society, 2015, 98(3): 758–769.